IEEE Access
Multidisciplinary ⋮ Rapid Review ⋮ Open Access Journal

Received 13 May 2024, accepted 8 June 2024, date of publication 21 June 2024, date of current version 16 July 2024.

Digital Object Identifier 10.1109/ACCESS.2024.3417484

RESEARCH ARTICLE

Adaptive State Feedback Shared Control for Unmanned Surface Vehicle With Fixed-Time Prescribed Performance Control

MENGYUE HE[1], CHAOBO LI[1], HUA HUANG[2], FANGFANG ZHOU[1], YUHANG HE[1], AND WEI SHANG[1,3,4]

[1]School of Mechanical Engineering, Hubei University of Technology, Wuhan 430068, China
[2]Wuhan Railway Vocational College of Technology, Wuhan 430074, China
[3]School of Mechanical Engineering and Mechanics, Ningbo University, Zhejiang 315211, China
[4]Ningbo Cixing Company Ltd., Ningbo 315000, China

Corresponding author: Huang Hua (Huanghua@wru.edu.cn)

ABSTRACT Unmanned surface vehicles (USVs) often encounter unknown obstacles, adverse weather, and emergency situations during missions, especially external disturbances such as wind, waves, and ocean currents at sea, which pose challenges for operators to respond promptly. To solve this issue, a Fixed-time prescribed performance adaptive state feedback shared control method for unmanned surface vehicles is proposed in this paper. The method comprises two parts: autonomous control based on Fixed-time prescribed performance adaptive state feedback for unmanned surface vehicles and shared control with adaptive state feedback, combining direct control commands with autonomous control. To ensure the convergence of tracking errors, a predefined performance control function is designed to guarantee transient error of the tracking error. Subsequently, an error transformation function is introduced for convenient controller design, and a nonlinear filter is used to compensate for boundary errors. Finally, utilizing the backstepping method, a controller is designed, and a Lyapunov function is formulated to verify the stability of unmanned surface vehicles using the designed transformation error. A state feedback shared control function is also designed to implement the shared control algorithm. Experimental results demonstrate the feasibility and effectiveness of this approach.

INDEX TERMS Unmanned surface vehicles, fixed-time prescribed performance control (FTPPC), adaptive control.

I. INTRODUCTION

In recent years, with the increasing demand for ocean exploration, USV control has become a hot topic in the industry. Currently, USVs are widely utilized in complex tasks such as ocean exploration, maritime rescue, and maritime patrols [1], [2], [3]. Operators can efficiently perform maritime tasks through remote operating systems. However, in the face of sudden situations, human operators may have difficulties reacting promptly, leading to potential risks like collisions. This significantly reduces the safety of unmanned maritime operations. Therefore, exploring an approach that combines direct human control with autonomous control of unmanned surface vehicles is essential to enhance their adaptability in complex environments.

In the field of unmanned control, shared control typically refers to the strategy of switching control authority between human operators and automatic control systems. During routine task execution, human operators are responsible for operating unmanned surface vehicles. At the same time, an adaptive state feedback controller comes into play in unexpected situations, such as when the unmanned surface vehicles encounters obstacles. This approach ensures efficient human operation while enabling timely responses in the face of danger. Currently, shared control finds widespread applications in the field of unmanned control. In [4],

The associate editor coordinating the review of this manuscript and approving it for publication was Min Wang.

a shared control framework considering the time-varying characteristics of the driver is proposed to enhance the safety of human-machine collaborative control, improving cooperative performance and mitigating risks associated with human-machine conflicts. In [5], a human-machine shared control method is introduced, allocating transmitted control coefficients reasonably based on mutual trust between humans and machines and environmental information. This strategy effectively enhances the operational efficiency of coal mine rescue robots. In [6], a novel cooperative control algorithm for Vehicle Manipulator (VM) and human operators is presented to optimize sensors for environmental perception and mechanical arm status measurement. However, there is currently a need for more sufficient research outcomes on shared control in unmanned vehicle control. Additionally, the control methods mentioned above mostly rely on fuzzy control, which poses challenges in terms of high computational complexity, long convergence times, and difficulty meeting high-precision control requirements.

To address the deficiencies mentioned above, there have been research outcomes in the field of unmanned surface vehicles [7], [8], [9]. To enhance the stability of unmanned surface vehicles in extreme environments, literature [8] proposes a finite-time disturbance observer and finite-time backstepping control method, ensuring the global strength of the system. In [9], a method is proposed to achieve trajectory tracking for unmanned surface vehicles in complex environments by combining non-singular fast terminal sliding mode and finite-time disturbance observer.However, in practical applications, if the initial state of the unmanned surface vehicle is far from the target point or the desired trajectory when starting a mission, finite-time control may require an extended duration for the unmanned surface vehicle to converge from the initial state to the target state. This could significantly impact the efficiency of the unmanned surface vehicle in executing tasks. To address this issue, a fixed-time convergence method has been introduced [10], [11], [12]. In [10], for tracking a single fully actuated Autonomous Surface Vehicle (ASV) trajectory, a controller based on a fixed-time state observer is proposed. Zhang J tackles the precise tracking problem of unmanned surface vehicles with external disturbances using a fixed-time disturbance observer, improving the tracking performance [11]. In [12], a practical event-triggered adaptive timed fuzzy controller is proposed based on backstepping techniques and timed stability theory. This controller is designed to eliminate the influence of the unmanned surface vehicle's initial state on convergence time. In the [23], a fixed-time distributed cooperative control strategy under actuator faults and input saturation constraints is designed for multiple surface vessels (MSVs), which enables the achievement of practical fixed-time stability.

It is worth noting that the research mentioned above focuses solely on steady-state performance, neglecting transient performance (i.e., overshoot and convergence speed). In reality, ensuring that the cooperative control system of unmanned surface vehicles achieves specified convergence performance in the uncertain marine environment is highly challenging. In the literature [22], a fixed-time sliding mode time-varying formation control strategy is proposed for multiple surface vessels (MSVs), which effectively enhances the performance of MSVs' formation control. However, the strategy does not explicitly emphasize satisfying predefined performance requirements during the control process, such as limiting overshoot or reducing steady-state errors. In [24], an event-triggered fixed-time distributed output feedback sliding mode cooperative control method is proposed to address a series of issues in the cooperative control of multiple surface vessels (MSVs), which ensures the practical fixed-time stability of the cooperative control system while considering input saturation. literature [13] first proposed a method of prescribed performance control (PPC), which, through defined performance functions and error transformations, can meet the requirements of fast convergence, slight overshoot, and minimal steady-state error. This control method has found extensive applications in unmanned surface vehicles. In [14], to address model uncertainties and time-varying external disturbances in unmanned surface vehicles, introduces an adaptive neural tracking control where prescribed performance control avoids singularity issues. In literature [15], a novel adaptive defined performance control strategy that achieves prescribed performance trajectory tracking while preventing the occurrence of discontinuous control signals is presented. In literature [16], Shen Z addresses trajectory tracking issues for USVs with full-state and input constraints, proposing a new prescribed performance and full-state constraint dynamic surface control scheme where the difined performance function ensures that the ship position tracking error meets requirements. In [25], the distributed cooperative control problem for multiple surface vessels (MSVs) under complex environments is investigated. By designing an observer and control algorithm, the cooperative control of MSVs is achieved, and the convergence of the cooperative errors within a fixed time is ensured. In literature [20], the authors introduced a neural adaptive dynamic surface asymptotic tracking control method, which achieved rapid convergence, slight overshoot, and minimal steady-state error requirements by defining performance functions and error transformations. In literature [21], researchers employed command filtering and adaptive control techniques to effectively handle time-varying parameters and input delays in the system, thereby achieving precise tracking control of the system. However, a common drawback of the above literature is the absence of provided convergence times.

Considering the limitations in current research within the unmanned surface vehicle domain, we have investigated an adaptive state feedback shared control method for unmanned surface vehicles with Fixed-time prescribed performance. In comparison to previous work, this approach offers the following advantages:

1. To address the challenges faced by operators of unmanned surface vessel (USV) formations in responding to unexpected situations, a shared control strategy is introduced, enhancing the safety of USV formations. This represents a novel contribution to the field of USV formation control research.

2. This paper proposes a Finite-Time Terminal Parallel Control (FTTPC) method capable of constraining tracking errors within specified performance bounds and achieving objectives within fixed time, providing a more comprehensive consideration of control issues compared to previous studies.

3. In comparison to prior research, the approach presented in this paper renders the stabilization time independent of initial conditions and unknown weights, yielding more accurate stabilization times. Simultaneously, by utilizing a performance function, the system ensures convergence of tracking errors to predefined performance bounds within fixed time, thereby further enhancing control effectiveness.

II. PROBLEM DESCRIPTION

A. MODEL DESCRIPTION

In this paper, the USV model based on the following mathematical models is established:

$$\begin{cases} \dot{x} = u\cos\varphi - v\sin\varphi \\ \dot{y} = u\sin\varphi + v\cos\varphi \\ \dot{\varphi} = r \end{cases} \tag{1}$$

where (x, y) represents the coordinates of an unmanned surface vessel, u, v represent the longitudinal linear velocity and transverse linear velocity of unmanned surface vessels, respectively; The yaw angle of an USV is denoted by φ, and r is the yaw rate. Meanwhile, a motion model for USV is described as follow:

$$\begin{cases} \dot{\boldsymbol{\eta}} = J(\boldsymbol{\eta})\boldsymbol{V} \\ M\dot{\boldsymbol{V}} + C\boldsymbol{V} + D\boldsymbol{V} = \boldsymbol{\tau} \end{cases} \tag{2}$$

In order to describe the following quantity conveniently, make $\boldsymbol{\eta} = [x \quad y \quad \varphi]^T, \boldsymbol{V} = [u \quad v \quad r]^T$; M represents inertia matrix in inertial coordinate system. C represents Coriolis and centripetal force matrix. D represents hydrodynamic damping matrix. The expression of them are as follows:

$$M = \begin{bmatrix} m_{11} & 0 & 0 \\ 0 & m_{22} & m_{23} \\ 0 & m_{32} & m_{33} \end{bmatrix} \tag{3}$$

$$C = \begin{bmatrix} 0 & 0 & -m_{22}v - m_{23}r \\ 0 & 0 & m_{11}u \\ m_{22}v + m_{23}r & -m_{11}u & 0 \end{bmatrix} \tag{4}$$

$$D = \begin{bmatrix} d_{11} & 0 & 0 \\ 0 & d_{22} & d_{23} \\ 0 & d_{32} & d_{33} \end{bmatrix} \tag{5}$$

In equation (2),$\boldsymbol{\tau} = [\boldsymbol{\tau}_u \quad \boldsymbol{\tau}_v \quad \boldsymbol{\tau}_r]^T$,where $\boldsymbol{\tau}_u$, $\boldsymbol{\tau}_v$ and $\boldsymbol{\tau}_r$ stand for longitudinal thrust, lateral thrust and turning moment of the ship respectively. And $\boldsymbol{\tau}$ is the control input of the unmanned surface vehicle. Based on the motion model of unmanned ship, the unmanned ship model used in this article as follows:

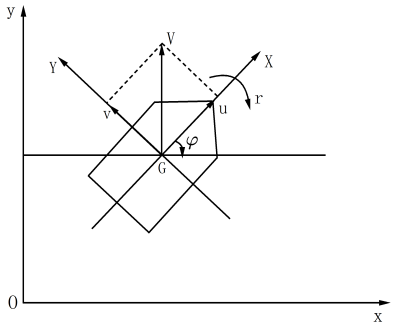

FIGURE 1. Single ship motion model.

$$\begin{cases} \dot{\boldsymbol{\eta}} = J(\boldsymbol{\eta})\boldsymbol{V} \\ \dot{\boldsymbol{V}} = M'\boldsymbol{\tau} - M'(C\boldsymbol{V} + D\boldsymbol{V}) \end{cases} \tag{6}$$

where $M' = M^{-1}$.

Control Objectives: This article presents performance control with adaptive fixed time regulation FTPPC algorithm is presented. Its control objectives are:

(1) Within a predetermined time frame, the specified reference signal η_d can be effectively tracked by the system output signal $\boldsymbol{\eta}$.

(2) The tracking and virtual errors consistently remain within predefined performance boundaries, converging to the expected steady-state error boundary within a predetermined time.

B. CONTROL PERFORMANCE FUNCTION (FTPPF)

To constrain the tracking error within a predetermined performance range over a fixed duration, we introduce FTPPF, denoting the Error Transformation Function (ETF):

Definition 1: If the function $\psi_i(t)$ belongs to FTPPF, it possesses the following distinctive characteristics:

1. $\psi_i(t)$ is a positive, smoothly decreasing, monotonous function;

2. As t approaches $\tilde{T}_i$, $\lim_{t\to\tilde{T}_i} \psi_i(t) = \psi_{\tilde{T}_i}$, where $\psi_{\tilde{T}_i}$ is any small positive real number.

3. When $\forall t \geq \tilde{T}_i$, $\psi_i(t) = \psi_{\tilde{T}_I}$, with $\tilde{T}_i$ representing sedimentation time.

In accordance with the aforementioned definition:

$$\psi_i(t) = \begin{cases} \left(\psi_{i,0}^{a_i} - a_i\lambda_i t\right)^{1/a_i} + \psi_{\tilde{T}_i} & 0 \leq t \leq \tilde{T}_i \\ \psi_{\tilde{T}_i} & \tilde{T}_i \leq t \end{cases} \tag{7}$$

where $\psi_{i,0} > 0, a_i > 0, \lambda_i > 0, \psi_{\tilde{T}_i} > 0$ are all design parameters, $a_i = \frac{p_i}{d_i}, d_i \geqslant p_i$ and $p_i > 0, d_i > 0$, are odd numbers and integers, respectively. In addition, $\psi_i(0) = \psi_{i,0} + \psi_{\tilde{T}_I}$ is initial error boundary. $\tilde{T}_i = \frac{{\psi_{i,0}}^{a_i}}{a_i\lambda_i}$ is settlement time. $\psi_{\tilde{T}_i} = \lim_{t\to\tilde{T}_i} \psi_i(t)$is steady-state error boundary.

Remark 1: Based on the requirement of control objectives (2) and the above definition, it is necessary to establish

$-\psi_i(t) \leq e_i(t) \leq \psi_i(t)$ when $t \geq 0$. Consequently, it is demanded that there is a large initial error boundary $\psi_i(0)$ to meet with $\psi_i(0) \geq e_i(0)$. It is assuming that $\psi_i(0) = \psi_{i,0} + \psi_{\tilde{T}_i}$, where $\psi_{\tilde{T}_i}$ is steady-state error boundary, requirement to guarantee the tracking error of the reference signal is limited within the specified performance boundary with a large design parameter $\psi_{i,0}$ appropriately. Meanwhile, it requests to achieve the expected control accuracy.

Definition 2: If the function $\Psi_i(\varepsilon_i(t))$ has the following three unique attributes:

1. $\Psi_i(\varepsilon_i(t))$ is a smooth strictly increasing function;
2. $-1 < \Psi_i(\varepsilon_i(t)) < 1$;
3.

$$\lim_{\varepsilon_i(t)\to+\infty} \Psi_i(\varepsilon_i(t)) = 1$$
$$\lim_{\varepsilon_i(t)\to-\infty} \Psi_i(\varepsilon_i(t)) = -1 \tag{8}$$

Then, ETF could be expressed as $\Psi_i(\varepsilon_i(t))$, where $\varepsilon_i(t)$ is error after conversion.

From the above definition, $\Psi_i(\varepsilon_i(t))$can express as follows:

$$\Psi_i(\varepsilon_i(t)) = \frac{2}{\pi}\arctan(\varepsilon_i(t)) \tag{9}$$

Therefore, the error is defined as follow:

$$e_i = \psi_i(t)\,\Psi_i(\varepsilon_i(t)) \tag{10}$$

Remark 2: The above definition of error clarifies the relationship among tracking errore_η, virtual errore_V, and conversion error ε_i,and by combining equation (9) and equation (10), it is known that $\varepsilon_i(t) = \tan\frac{\pi e_i(t)}{2\psi_i(t)}$. In addition, it can be got from $-1 < \Psi_i(\varepsilon_i(t)) < 1$ and $\psi_i(t) > 0$ that $-\psi_i(t) < e_i = \psi_i(t)\,\Psi_i(\varepsilon_i(t)) < \psi_i(t)$.Therefore, We can make a decision, when satisfying $\psi_i(0) \geq e_i(0)$, the control objective can be achieved through ETF.

C. ERROR CONVERSION

A new dynamic model is defined based on the following coordinate transformation, which is the innovation of this article:

$$\boldsymbol{e}_\eta = \boldsymbol{\eta} - \eta_d \tag{11}$$
$$\boldsymbol{e}_V = \boldsymbol{V} - \alpha_\eta^{\mathrm{c}} \tag{12}$$

Next, taking the derivative of time yields:

$$\dot{\boldsymbol{e}}_\eta = J(\boldsymbol{\eta})\boldsymbol{V} - \dot{\eta}_d \tag{13}$$
$$\dot{\boldsymbol{e}}_V = M'\boldsymbol{\tau} - M'(C\boldsymbol{V} + D\boldsymbol{V}) - \dot{\alpha}_\eta^{\mathrm{c}} \tag{14}$$

According to equation (10) we can get:

$$\dot{\boldsymbol{e}}_i = \dot{\psi}_i(t)\,\Psi_i(\varepsilon_i(t)) + \psi_i(t)\frac{\partial\Psi_i(\varepsilon_i(t))}{\partial\varepsilon_i(t)}\dot{\varepsilon}_i(t) \tag{15}$$

where $\phi_i(\varepsilon_i(t), \psi_i(t)) = -\frac{\dot{\psi}_i\Psi_i(\varepsilon_i(t))}{\psi_i\frac{\partial\Psi_i(\varepsilon_i(t))}{\partial\varepsilon_i(t)}}$, $\xi_i(\varepsilon_i(t), \psi_i(t)) = \frac{1}{\psi_i\frac{\partial\Psi_i(\varepsilon_i(t))}{\partial\varepsilon_i(t)}}$, $i = \boldsymbol{\eta}, \boldsymbol{V}$.

As defined above, the state equation of the system (1) is rewritten as:

$$\begin{cases} \dot{\varepsilon}_\eta = \phi_\eta + \xi_\eta(J(\boldsymbol{\eta})\boldsymbol{V} - \dot{\eta}_{\mathrm{d}}) \\ \dot{\varepsilon}_V = \phi_V + \xi_V\left(M'\boldsymbol{\tau} - M'(C\boldsymbol{V} + D\boldsymbol{V}) - \dot{\alpha}_\eta^{\mathrm{c}}\right) \end{cases} \tag{16}$$

Remark 3: This paper establishes a predefined performance mechanism within a fixed time framework. Typically, both the virtual error $\boldsymbol{e}_V$ and the tracking error $\boldsymbol{e}_\eta$ are constrained by the designed prescribed performance function $\psi i(t)$. However, in equation [22], the limitation is applied solely to the tracking error e_η within the specified performance function range. Furthermore, by applying (11) to (12), we derive $-\psi_\eta(t) + \eta_d < \boldsymbol{\eta} < \psi_\eta(t) + \eta_d$ and $-\psi_V(t) + \alpha_\eta^c < \boldsymbol{V} < \psi_V(t) + \alpha_\eta^c$. It can be concluded that the system state $\boldsymbol{\eta}, \boldsymbol{V}$ is bounded.

D. SHARED CONTROL INPUT

The kinematic model of a single USV in this paper is described as follow:

$$M\dot{\boldsymbol{V}} + C\boldsymbol{V} + D\boldsymbol{V} = \boldsymbol{u}_{\mathrm{s}} \tag{17}$$

Symbols: S (t) is a fixed-time set.$\boldsymbol{u}_s(\boldsymbol{u}_h, \boldsymbol{\tau}) \in \mathbb{R}^n$ represents the generalized control input function about the input applied by the operator $\boldsymbol{u}_h$ and the input applied by the feedback controller $\boldsymbol{\tau}$.

Assumption 1: A nonempty feasible set P_a is defined by a set of linear inequalities, namely:

$$P_a = \left\{\boldsymbol{\eta} \in \mathbb{R}^n / S\boldsymbol{\eta} + T \leqslant 0\right\} \tag{18}$$

If $\boldsymbol{S} = \left[\boldsymbol{s}_1^{\mathrm{T}}, \boldsymbol{s}_2^{\mathrm{T}}, \ldots, \boldsymbol{s}_{\mathrm{m}}^{\mathrm{T}}\right]^{\mathrm{T}} \in \mathbb{R}^{m\times n}$, $T = [t_1, t_2, \ldots, t_m]^{\mathrm{T}} \in \mathbb{R}^m$ and $T = [t_1, t_2, \ldots, t_m]^{\mathrm{T}} \in \mathbb{R}^m$, where $\mathrm{s}_i \in \mathbb{R}^n$, $t_i \in \mathbb{R}$, $i \in \{1, 2, \ldots, m\}$. In the case of $m > n$, the matrices S and T must satisfy the condition $\mathrm{rank}(\left[\boldsymbol{s}_{r1}^{\mathrm{T}}, \boldsymbol{s}_{r2}^{\mathrm{T}}, \ldots, \boldsymbol{s}_{rl}^{\mathrm{T}}\right]^{\mathrm{T}}) < \mathrm{rank}(\left[\boldsymbol{h}_{r1}^{\mathrm{T}}, \boldsymbol{h}_{r2}^{\mathrm{T}}, \ldots, \boldsymbol{h}_{rl}^{\mathrm{T}}\right]^{\mathrm{T}})$, where $\boldsymbol{h}_{\mathrm{ri}} = \left[\boldsymbol{s}_{ri}^{\mathrm{T}}, \mathrm{t}_{ri}^{T}\right]$ for $i \in \{1, 2, \ldots, l\}$, $r_1, r_2, \ldots, r_l \in \{1, 2, \ldots, m\}$, and $l \in [n+1, m]$.

Definition 3: If there exists $k > 0$ such that $\boldsymbol{s}_j^{\mathrm{T}}(\boldsymbol{\eta} + k\boldsymbol{V}) + t_j = 0$, then the jth velocity $\boldsymbol{V} \in \mathbb{R}^n$ is effective.

Lemma 1: Given the set P_a and the satisfaction of Assumption 1, it can be concluded that, for any fixed $\boldsymbol{V} \in \mathbb{R}^n$, the number of violated constraints does not exceed n.

Remark 4: According to Lemma 1, the m linear inequality constraints can be organized into groups denoted as N_c. In the case of $m \geqslant n$, generally, $N_c \leqslant \left(m\,n\right)$. If $m < n$, then $N_c = 1$. Within each group, there are n constraint conditions. It is evident that if $m \geqslant n$ holds true, as Lemma 1 suggests.If $m < n$, each group contains n constraints is satisfied.

Definition 4: Utilizing the velocity and distance to the boundary, the overall state velocity can be categorized into three subspaces: the safe set R_s, the hysteresis set R_h, and the dangerous set R_d. In connection with the ith group of active constraints:

$$\boldsymbol{x}^i = S^i\boldsymbol{\eta} + T^i \leqslant 0 \tag{19}$$

utilizing $T^i \in \mathbb{R}^n$ and S^i, the definitions of the safe, hysteresis, and dangerous subsets can be described as:

$$\begin{aligned}
\bar{\Re}_s &= \Big\{(\boldsymbol{x}^i, \dot{\boldsymbol{x}}^i) \in \chi_a^i \times \mathbb{R}^n : \dot{x}_j^i \le \frac{1}{x_j^i + b_2} - \frac{1}{b_2}, \\
&\quad \text{if } x_j^i \ge -b_2, \forall j \in \{1, 2, \ldots, n\}\Big\} \\
\bar{\Re}_h &= \Big\{(\boldsymbol{x}^i, \dot{\boldsymbol{x}}^i) \in \chi_a^i \times \mathbb{R}^n : \exists j \in \{1, 2, \ldots, n\} \\
&\quad \text{such that } \dot{x}_j^i > \frac{1}{x_j^i + b_2} - \frac{1}{b_2}, x_j^i \ge -b_2, \\
&\quad \text{and } \dot{x}_k^i < \frac{1}{x_k^i + b_1} - \frac{1}{b_1}, \\
&\quad \text{if } \dot{x}_k^i \ge -b_1, \forall k \in \{1, 2, \ldots, n\}\Big\} \\
\bar{\Re}_d &= \Big\{(\boldsymbol{x}^i, \dot{\boldsymbol{x}}^i) \in \chi_a^i \times \mathbb{R}^n : \exists j \in \{1, 2, \ldots, n\} \\
&\quad \text{such that } \dot{x}_j^i \ge \frac{1}{x_j^i + b_1} - \frac{1}{b_1}, \\
&\quad -b_1 \le x_j^i < 0\Big\}
\end{aligned} \tag{20}$$

where $\chi_a^i = S^i P_a + T^i, b_2 > b_1 > 0$.

Definition 5: The s-closed-loop system and h-closed-loop system are described by (17) and $\dot{\boldsymbol{M}}\boldsymbol{V} + \boldsymbol{C}\boldsymbol{V} + \boldsymbol{D}\boldsymbol{V} = \boldsymbol{u}_h$, respectively. Additionally, use Ω_h, Ω_s to represent the Ω-limit sets of both the h-closed-loop and s-closed-loop systems.

Assumption 2: Assuming full states $\boldsymbol{\eta}(t)$ and $\boldsymbol{V}(t)$ can be used for measurement. Assuming the required configuration is designed to ensure the existence of $\eta_d(t) \in \mathbb{R}^n$ and is bounded.

Assumption P_a represents a given and compact feasible configuration set for the system (17), with $\boldsymbol{u}_h$ as a predefined artificial input.Design feedback controllers, safe subsets, and shared functions that satisfy the following properties:

1) The system consistently maintains its configuration within the set P_a, and a safe subset $\Re_s \subset \Re$ is defined specifically for the system. Here, $\Re \triangleq P_a \times \mathbb{R}^n$ stands as a forward-invariant set.

2) $\boldsymbol{u}_s$ cannot alter the goal of human operator's, namely, Ω_s, Ω_h are $\Omega -$ limit sets of the closed-loop system, with shared control input by both $\boldsymbol{u}_s$ and the human operator $\boldsymbol{u}_h$: if $\Omega_h \subset \Re_s$, then $\boldsymbol{u}_s = \boldsymbol{u}_h$; if $\Omega_h \not\subset \Re_s$, then $\Omega_s = \Pi_{\Re_s}(\Omega_h)$.

3) If the system's state remains in the safe subset, then $\boldsymbol{u}_s = \boldsymbol{u}_h$.

III. CONTROL DESIGN

A. DESIGN OF NONLINEAR FILTER

Nonlinear filters can provide stronger robustness, namely the ability to adapt to changes in system parameters or external disturbances. This is crucial for control systems facing uncertainty. In the control design section, it is necessary to use the nonlinear filter to achieve the dynamic surface control technology. The design is as follows:

$$\begin{aligned}
\tau_i \dot{\alpha}_i^c &= -\left(1 + \frac{\tau_i}{2}\right)\omega_i - \tau_i \hat{\kappa}_i \tanh\left(\frac{\hat{\kappa}_i \omega_i}{m_i}\right) \\
\alpha_i^c(0) &= \alpha_i(0)
\end{aligned} \tag{21}$$

where $\tau_i > 0, (i = \eta, V)$ is the design parameter of nonlinear filter, and α_i^c is a novel designed variable, α_i is the virtual control signal. $\omega_i = \alpha_i^c - \alpha_i$ indicates the boundary layer error. Make an assumption that κ_i' is the upper boundary of $|\dot{\alpha}_i|$, and make a definition that $\hat{\kappa}_i' = \kappa_i' - \hat{\kappa}_i$ is estimation error, where $\hat{\kappa}_i$ is the estimated value of κ_i'.

Consequently, the adaptive update law of $\hat{\kappa}_i$ can be defined as:

$$\dot{\hat{\kappa}}_i = b_i|\omega_i| - \bar{b}_i \hat{\kappa}_i, \quad \hat{\kappa}_i(0) \ge 0. \tag{22}$$

where $b_i > 0$ and $\bar{b}_i > 0$.

Proposition 1: In formula (21), the adaptive parameter $\hat{\kappa}_i(0) \ge 0$ always on account of the adaptive update law (22) when $\hat{\kappa}_i \ge 0$.

Proof: In (22), it is known that $\hat{\kappa}_i$ is continuous over time t. Assuming there is a certain moment of motion $t_2 > 0$ that $\hat{\kappa}_i(t_2) < 0$ and combining the initial message $\hat{\kappa}_i(0) \ge 0$ from (22), there must be a certain moment of motion $t_1 \in (0, t_2]$, as follows:

$$\begin{cases}
\hat{\kappa}_i(t_1) = 0 \\
\hat{\kappa}_i(t) < 0, t \in (t_1, t_2]
\end{cases} \tag{23}$$

Consequently, according to the definition of $\dot{\hat{\kappa}}_i$, the inequality $\dot{\hat{\kappa}}_i(t) > 0$ always can be satisfied when $t \in (t_1, t_2]$. Integrate $\dot{\hat{\kappa}}_i$ from t_1 to t_2 yields

$$\int_{t_1}^{t_2} \dot{\hat{\kappa}}_i(t)\, dt = \hat{\kappa}_i(t_2) - \hat{\kappa}_i(t_1) = \hat{\kappa}_i(t_2) > 0. \tag{24}$$

But this contradicts our hypothesis of $\hat{\kappa}_i(t_2) < 0$. Therefore, get to a conclusion that $\hat{\kappa}_i(t) \ge 0$ holds for $\forall t > 0$.

Remark 5: A nonlinear filter with an adaptive parameter estimator is designed in this article. Different from traditional linear filters, the nonlinear filter eases the requirements for filter design parameter τ_i and reimburses for boundary layer errors. DSC technology based on nonlinear filters can validly solve the problem of explosion of computational complexity. In addition, including nonlinear filters in the proposed DSC technology can in the control project compensate for bounding layer errors.

B. DESIGN OF ADAPTIVE FTPPC

Throughout the adaptive FTPPC design, the following coordinate transformations are applied:

$$\begin{cases}
z_\eta = \boldsymbol{\varepsilon}_\eta \\
z_V = \boldsymbol{\varepsilon}_V \\
\omega_\eta = \alpha_\eta^c - \alpha_\eta
\end{cases} \tag{25}$$

Step 1: Taking the derivative of z_η yields:

$$\dot{z}_\eta = \xi_\eta \left(\xi_\eta^{-1}\phi_\eta + J(\boldsymbol{\eta})\boldsymbol{e}_V + J(\boldsymbol{\eta})\alpha_\eta + J(\boldsymbol{\eta})\omega_\eta - \dot{\eta}_\mathrm{d}\right) \tag{26}$$

where $\boldsymbol{e}_V = \frac{2}{\pi}\psi_V \arctan(z_V)$.

The selection of Lyapunov function is as follows:

$$V_\eta = \frac{k_\eta^2}{\pi \xi_\eta} \tan\left(\frac{\pi z_\eta^2}{2k_\eta^2}\right) \tag{27}$$

where $k_\eta > 0, \xi_\eta > 0$ are design parameters.

Remark 6: Based on the Tan-type Barrier Lyapunov Function in [17], a novel Lyapunov function in (27) is introduced. Limit the transformation error ε_i to a given constant boundary k_i and get an inequality $|\varepsilon_i| < k_i$ when $z_i = \varepsilon_i$. It is worth mentioning that this article implements constraints on both state tracking error and transformation error simultaneously. Furthermore, it is to be noted that the design parameter k_i should be appropriately selected to make $k_i \geqslant \varepsilon_i(0) = \tan\frac{\pi e_i(0)}{2\psi_i(0)}$ holds, given $\varepsilon_i(t) = \tan\frac{\pi e_i(t)}{2\psi_i(t)}$.

Consequently, from (26) and (27), get that:

$$\begin{aligned}\dot{V}_\eta &= -\frac{k_\eta^2 \dot{\xi}_\eta}{\pi \xi_\eta^2} \tan\left(\frac{\pi z_\eta^2}{2k_\eta^2}\right) + \frac{z_\eta \dot{z}_\eta}{\xi_\eta \cos^2\left(\frac{\pi z_\eta^2}{2k_\eta^2}\right)} \\ &= \upsilon_\eta z_\eta \left(\xi_\eta^{-1}\phi_\eta + J(\eta)e_V + J(\eta)\alpha_\eta + J(\eta)\omega_\eta - \dot{\eta}_d\right) \\ &\quad + \frac{k_\eta^2 \dot{\psi}_\eta \left(1 + z_\eta^2\right)}{2\psi_\eta^2 \xi_\eta^2} \tan\left(\frac{\pi z_\eta^2}{2k_\eta^2}\right)\end{aligned} \tag{28}$$

where $\upsilon_\eta = \frac{1}{\cos^2}\left(\frac{\pi z_\eta^2}{2k_\eta^2}\right) - \frac{k_\eta^2}{\xi_\eta \psi_\eta} \tan\left(\frac{\pi z_\eta^2}{2k_\eta^2}\right)$.

By using Young's inequality, it can be expressed as:

$$\upsilon_\eta z_\eta J(\boldsymbol{\eta})\left(\boldsymbol{e}_V + \omega_\eta\right) \leq \upsilon_\eta^2 z_\eta^2 (J(\boldsymbol{\eta}))^2 + \frac{1}{2}\boldsymbol{e}_V^2 + \frac{1}{2}\omega_\eta^2 \tag{29}$$

From (28) and (29), get that:

$$\begin{aligned}\dot{V}_\eta &\leq \upsilon_\eta z_\eta \left(\xi^{-1}\phi_\eta + J(\boldsymbol{\eta})\alpha_\eta - \dot{\eta}_\mathrm{d} + \upsilon_\eta z_\eta (J(\boldsymbol{\eta}))^2\right) \\ &\quad + \frac{1}{2}\boldsymbol{e}_V^2 + \frac{1}{2}\omega_\eta^2 + \frac{k_\eta^2 \dot{\psi}_\eta \left(1 + z_\eta^2\right)}{2\psi_\eta^2 \xi_\eta^2} \tan\left(\frac{\pi z_\eta^2}{2k_\eta^2}\right)\end{aligned} \tag{30}$$

Select virtual control function α_η:

$$\begin{aligned}\alpha_\eta &= (J(\boldsymbol{\eta}))^{-1} \begin{bmatrix} -\frac{l_\eta}{z_\eta \xi_\eta} \sin\left(\frac{\pi z_\eta^2}{2k_\eta^2}\right)\cos\left(\frac{\pi z_\eta^2}{2k_\eta^2}\right) \\ -\frac{l_\eta k_\eta^2}{\upsilon_\eta z_\eta \xi_\eta^2 \psi_\eta} \sin^2\left(\frac{\pi z_\eta^2}{2k_\eta^2}\right) - \xi_\eta^{-1}\phi_\eta \\ -\frac{k_\eta^2 \dot{\psi}_\eta}{2\upsilon_\eta z_\eta \psi_\eta^2 \xi_\eta^2} \tan\left(\frac{\pi z_\eta^2}{2k_\eta^2}\right) \\ -\frac{k_\eta^2 \dot{\psi}_\eta z_\eta}{2\upsilon_\eta \psi_\eta^2 \xi_\eta^2} \tan\left(\frac{\pi z_\eta^2}{2k_\eta^2}\right) + \dot{\eta}_d - \upsilon_\eta z_\eta (J(\boldsymbol{\eta}))^2 \end{bmatrix}\end{aligned} \tag{31}$$

where $l_\eta > 0$ is design parameter.

Remark 7: In the suppositional regulatory function α_η, while the error variable z_η is located on the denominator, there is still no singularity phenomenon. The L'Hospital rule can be used to explain this conclusion:

$$\begin{aligned}&\lim_{z_\eta \to 0} \frac{l_\eta}{z_\eta \xi \eta} \sin\left(\frac{\pi z \eta^2}{2k_\eta^2}\right)\cos\left(\frac{\pi z \eta^2}{2k \eta^2}\right) = 0, \\ &\lim_{z_\eta \to 0} \frac{l_\eta k_\eta^2}{\upsilon_\eta z_\eta \xi_\eta^2 \psi_\eta} \sin^2\left(\frac{\pi z_\eta^2}{2k_\eta^2}\right) = 0, \\ &\lim_{z_\eta \to 0} \frac{k_\eta^2 \dot{\psi}_\eta}{2\upsilon_\eta z_\eta \psi_\eta^2 \xi_\eta^2} \tan\left(\frac{\pi z_\eta^2}{2k_\eta^2}\right) = 0.\end{aligned}$$

However, in actual implementation, a small boundary ς is raised, if $|z_\eta| < \varsigma$ is satisfied, the above terms are all equal to 0. Otherwise, the calculation of the above terms is normal and does not affect the control effect.

Substituting (31) into (30) yields:

$$\dot{V}_\eta \leq -\frac{l_\eta}{\xi_\eta} \tan\left(\frac{\pi z_\eta^2}{2k_\eta^2}\right) + \frac{1}{2}\boldsymbol{e}_V^2 + \frac{1}{2}\omega_\eta^2 \tag{32}$$

Step 2: ($i = \boldsymbol{V}$) (according to the backstepping method) From (16) and (25), the definition of $\dot{z}_V$ can be obtained:

$$\dot{z}_V = \xi_V \begin{bmatrix} \xi_V^{-1}\phi_V - M'(C\boldsymbol{V} + D\boldsymbol{V}) + M'\boldsymbol{\tau} \\ + \left(\frac{1}{\tau_\eta} + \frac{1}{2}\right)\omega_\eta + \hat{\lambda}_\eta \tanh\left(\frac{\hat{\lambda}_\eta \omega_\eta}{m}\right) \end{bmatrix} \tag{33}$$

Then the Lyapunov function is chosen as follows:

$$\begin{aligned}V_V &= V_\eta + \frac{k_V^2}{\pi \xi_V} \tan\left(\frac{\pi z_V^2}{2k_V^2}\right) \\ &\quad + \frac{1}{2\delta}(\tilde{M}')^T \tilde{M}' + \frac{1}{2}\omega_\eta^2 + \frac{1}{2b_\eta}(\tilde{\kappa}_\eta')^2\end{aligned} \tag{34}$$

where $k_V > 0, \xi_V > 0, \delta > 0$ are positive design parameters,$\hat{M}'$ is the estimated value of M' and $\tilde{M}' = M' - \hat{M}'$ is estimated error.

Then, the time-derivative of V_V is as shown below.:

$$\begin{aligned}\dot{V}_V &= \dot{V}_\eta - \frac{k_V^2 \dot{\xi}_V}{\pi \xi_V^2} \tan\left(\frac{\pi z_V^2}{2k_V^2}\right) + \frac{z_V \dot{z}_V}{\xi_V \cos^2\left(\frac{\pi z_V^2}{2k_V^2}\right)} - \frac{1}{\delta}\tilde{M'}^T \dot{\hat{M}}' \\ &\quad + \omega_\eta \dot{\omega}_\eta - \frac{1}{b_\eta}\tilde{\lambda'}_\eta \dot{\hat{\lambda}}_\eta \\ &\leq -\frac{l_\eta}{\xi_\eta} \tan\left(\frac{\pi z_\eta^2}{2k_\eta^2}\right) - \frac{1}{\tau_\eta}\omega_\eta^2 + \frac{\bar{b}_\eta}{b_\eta}\tilde{\lambda'}_\eta \hat{\lambda}_\eta \\ &\quad + \upsilon_V z_V \left(\xi_V^{-1}\phi_V - M'(C\boldsymbol{V} + D\boldsymbol{V})\right) \\ &\quad + M'\boldsymbol{\tau} + \frac{\boldsymbol{e}_V^2}{2\upsilon_V z_V} + \left(\frac{1}{\tau_\eta} + \frac{1}{2}\right)\omega_\eta + \tilde{\lambda}_\eta \tanh\left(\frac{\tilde{\lambda}_\eta \omega_\eta}{m}\right) \\ &\quad + \frac{k_V^2 \dot{\psi}_V \left(1 + z_V^2\right)}{2\psi_V^2 \xi_V^2} \tan\left(\frac{\pi z_V^2}{2k_V^2}\right) - \frac{1}{\delta}\tilde{M'}^T \dot{\hat{M}}' + 0.2785m\end{aligned} \tag{35}$$

where $\upsilon_V = \frac{1}{\cos^2\left(\frac{\pi z_V^2}{2k_V^2}\right)} - \frac{k_V^2}{\xi_V \psi_V} \tan\left(\frac{\pi z_V^2}{2k_V^2}\right)$.

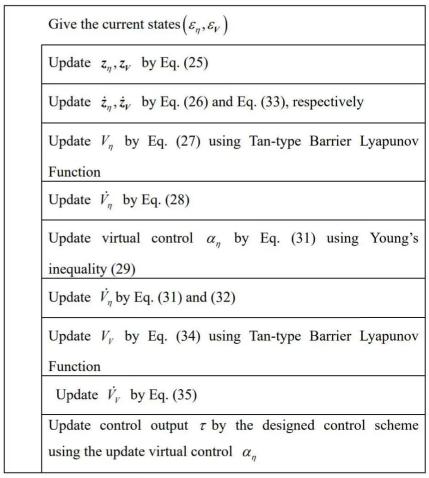

FIGURE 2. Nassi shneider man diagram for design of adaptive FTPPC.

Then, the definition of τ is represented as follows:

$$\boldsymbol{\tau} = \left(M'\right)^{-1}\begin{bmatrix} -\frac{l_V}{z_V\xi_V}\sin\left(\frac{\pi z_V^2}{2k_V}\right)^2\cos\left(\frac{\pi z_V^2}{2k_V}\right)^2 \\ -\frac{l_V {k_V}^2}{\upsilon_V z_V \xi_V^2 \psi_V}\sin^2\left(\frac{\pi z_V^2}{2k_V^2}\right) - \xi_V^{-1}\phi_V \\ -\frac{k_V^2\dot{\psi}_V}{2\upsilon_V z_V \psi_V^2 \xi_V^2}\tan\left(\frac{\pi z_V^2}{2k_V^2}\right) - \frac{\boldsymbol{e}_V^2}{2\upsilon_V z_V} \\ -\frac{k_V^2\dot{\psi}_V z_V}{2\upsilon_V \psi_V^2 \xi_V^2}\tan\left(\frac{\pi z_V^2}{2k_V^2}\right) + \hat{M'}^T(\boldsymbol{CV}+\boldsymbol{DV}) \\ -\left(\frac{1}{\tau_\eta}+\frac{1}{2}\right)\omega_\eta - \hat{\lambda}_\eta \tanh\left(\frac{\hat{\lambda}_\eta \omega_\eta}{m_V}\right) \end{bmatrix} \tag{36}$$

where

$$\dot{\hat{M}}' = -\rho\hat{M}' - \delta\upsilon_V z_V(\boldsymbol{CV}+\boldsymbol{DV}) \tag{37}$$

and $l_V > 0$, $\rho > 0$ are design parameters.

According to Remark 7, $\lim_{z_V\to 0}\frac{\boldsymbol{e}_V}{2\upsilon_V z_V} = 0$ can be obtained. Then, get that:

$$\dot{V}_V \leq -\left[\frac{\mathbf{l}_\eta}{\xi_\eta}\tan\left(\frac{\pi z_\eta^2}{2k_\eta^2}\right) + \frac{\mathbf{l}_V}{\xi_V}\tan\left(\frac{\pi z_V^2}{2k_V^2}\right)\right] + \frac{\rho}{\delta}\tilde{M'}^T\hat{M}' - \frac{1}{\tau_\eta}\omega_\eta^2 + \frac{\bar{b}_\eta}{b_\eta}\tilde{\lambda'}_\eta\hat{\lambda}_\eta + M_V \tag{38}$$

and $\mathrm{M}_V = 0.2785\mathrm{m}_V$.

C. STABILITY ANALYSIS

Theorem 1: For the control input(36), the virtual regulatory function(31), and the parameter adaptation laws(22),(37), the system (6) possesses the following characteristics: i) All signals are ultimately bounded and semi globally uniformly bounded; ii) All dynamic errors are predetermined bounded within a regular hour.

Proof:

$$V = V_V = \frac{k_\eta^2}{\pi\xi_\eta}\tan\left(\frac{\pi z_\eta^2}{2k_\eta^2}\right) + \frac{k_V^2}{\pi\xi_V}\tan\left(\frac{\pi z_V^2}{2k_V^2}\right) + \frac{1}{2\delta}\tilde{M'}^T\tilde{M}' + \frac{1}{2}\omega_\eta^2 + \frac{1}{2b_\eta}\tilde{\lambda'}_\eta^2 \tag{39}$$

where $\omega_\eta = 0, \tilde{\lambda}_\eta = 0$, then

$$\dot{V} \leq -\left[\frac{l_\eta}{\xi_\eta}\tan\left(\frac{\pi z_\eta^2}{2k_\eta^2}\right) + \frac{l_V}{\xi_V}\tan\left(\frac{\pi z_V^2}{2k_V^2}\right)\right] + \frac{\rho}{\delta}\tilde{M'}^T\hat{M}' - \frac{1}{\tau_\eta}\omega_\eta^2 + \frac{\bar{b}_\eta}{b_\eta}\tilde{\lambda'}_\eta\hat{\lambda}_\eta + M_V \tag{40}$$

using the Youngś inequality,

$$\frac{\rho}{\delta}\tilde{M'}^{\mathrm{T}}\hat{M}' \leqslant -\frac{\rho}{2\delta}\tilde{M'}^{\mathrm{T}}\tilde{M}' + \frac{\rho}{2\delta}M'^{\mathrm{T}}M' \tag{41}$$

$$\frac{\bar{b}_\eta}{b_\eta}\tilde{\kappa}'_\eta\hat{\kappa}_\eta \leq -\frac{\bar{b}_\eta}{2b_\eta}(\tilde{\kappa}'_\eta)^2 + \frac{\bar{b}_\eta}{2b_\eta}\kappa_\eta^2 \tag{42}$$

then

$$\dot{V} \leq -\left[\frac{l_\eta}{\xi_\eta}\tan\left(\frac{\pi z_\eta^2}{2k_\eta^2}\right) + \frac{l_V}{\xi_V}\tan\left(\frac{\pi z_V^2}{2k_V^2}\right)\right] - \frac{\rho}{2\delta}\tilde{M'}^T\tilde{M}' - \frac{1}{\tau_\eta}\omega_\eta^2 - \frac{\bar{b}_\eta}{2b_\eta}\tilde{\lambda'}_\eta^2 + \bar{M}_V \tag{43}$$

where $\bar{M}_V = M_V + \frac{\rho}{2\delta}M'^{\mathrm{T}}M' + \frac{\bar{b}_\eta}{2b_\eta}(\kappa'_\eta)^2$

then

$$\dot{V} \leqslant -cV + \lambda \tag{44}$$

where $c = \min\left\{\frac{\pi l_\eta}{k_\eta^2}, \frac{\pi l_V}{k_V^2}, \rho, \frac{2}{\tau_\eta}, \bar{b}_\eta\right\}, \lambda = \bar{M}_V$.

$$V_V \leqslant V \leqslant e^{-ct}\left(V(0) - \frac{\lambda}{c}\right) + \frac{\lambda}{c} \tag{45}$$

Given the boundedness of the expression (45) and the initial value of error variable $z_i(0), \tilde{M}'(0), \omega_i(0), \tilde{\kappa}'_i(0)$, it is inferred that the parameter estimation error $z_i, \tilde{M}', \omega_i, \tilde{\kappa}'_i$ remains within limits. Considering the bounded nature κ'_i and M', the estimated values for parameters $\hat{\kappa}_i$ and $\hat{M}'$ are also constrained. Consequently, with the Lyapunov function and the design of the error transformation mechanism associated with the barrier-type potential, it is established that the transformation error stays within a specified constant boundary. Simultaneously, the state tracking error is maintained within a small predefined range over a fixed time interval.

D. SHARED CONTROL LOW

In describing the n constraints of the i-th group, as outlined in (19), the state-space can be partitioned into three subcollections according to (20). To eliminate ambiguity between different constraint groups, $\Re_\zeta^i = diag\left(S^{i-1}, S^{i-1}\right)\left[\bar{\Re}_\zeta^i - col\left(T^i, 0\right)\right]$ must be employed,

where the $\zeta = \{s, h, d\}$ relation relocates these subsets back into the $(\boldsymbol{\eta}, \boldsymbol{V})$ coordinate system. Therefore, by constructing $\Re_s^i \cup \Re_h^i \cup \Re_d^i = \Re$ with $i \in \{1, 2, \ldots, N_c\}$, it shows that for the i-th group of active constraints, any fixed $\dot{\boldsymbol{\eta}}$ results in a union of safe, hysteresis, and dangerous sets that are consistent, in other words, $S^i \boldsymbol{\eta} + T^i \leq 0$ is consistent with the overall practicable state-space. Subsequently, the total safe, perilous, and hysteresis sets for different constraint groups are defined as $\Re_s = \Re_s^1 \cap \Re_s^2 \cap \ldots \cap \Re_s^{N_c}$, $\Re_d = \Re_d^1 \cup \Re_d^2 \cup \ldots \cup \Re_d^{N_c}$, $\Re_h = \Re - \Re_d - \Re_s$.

On account of these subaggregates, the shared control input $\boldsymbol{u}_s(\boldsymbol{\eta}, \boldsymbol{V})$ defined in the $(\boldsymbol{\eta}, \boldsymbol{V})$ coordinates is given by:

$$\boldsymbol{u}_s = \left(\min_{1 \leq i \leq N_c} k_{\mathrm{sf}}^i \right) \boldsymbol{u}_h + \sum_{i=1}^{N_c} \left[\left(1 - k_{\mathrm{sf}}^i \right) \boldsymbol{\tau} \right] \tag{46}$$

The shared control function of state feedback is:

$$k_{\mathrm{sf}}^i (\boldsymbol{\eta}, \boldsymbol{V}, t) = \begin{cases} 0 & \text{if } (\boldsymbol{\eta}, \boldsymbol{V}) \in \Re_d^i, \quad \boldsymbol{V}^i = \min\limits_{j=L1}^{L_{N_c}} \boldsymbol{V}^j \\ l_{\mathrm{sf}}^i & \text{if } (\boldsymbol{\eta}, \boldsymbol{V}) \in \Re_h^i \\ 1 & \text{otherwise} \end{cases} \tag{47}$$

where

$$l_{sf}^i = \begin{cases} 0 & k_{sf}^i \left(t^- \right) = 0 \\ 1 & k_{sf}^i \left(t^- \right) = 1 \end{cases} \tag{48}$$

Theorem 2: Given that system (17) with the shared control input provided by (46) with (36). Suppose the initialization meets the conditions $((\boldsymbol{\eta}(0), \boldsymbol{V}(0)) \in \mathbb{R}_s)$. Assume the existence of $\tilde{t} > 0$ such that $\tilde{\boldsymbol{\eta}}(t) \notin P_a$. Then, it exists $0 < t_d < \tilde{t}$ such that $((\boldsymbol{\eta}(t_d), \boldsymbol{V}(t_d)) \in \mathbb{R}_d)$

Proof: The assertion is due to definition of continuity and other aspects of trajectories, according to the statement of Theorem 1.

Theorem 3: Suppose the system (17) with $\boldsymbol{\eta}(0) \in P_a$. Consider the shared control input provided by (46) and (36). Then, the Closed loop system has the following features:

1) for all $t \geq 0$, $\boldsymbol{\eta}(t) \in P_a$;
2) $\Omega_s = \Pi_{\Re_s}(\Omega_h)$;
3) for all $t \geq 0$; $\boldsymbol{u}_s(t) = \boldsymbol{u}_h(t)$ and $(\boldsymbol{\eta}(t), \boldsymbol{V}(t)) \in \Re_s$;

Remark 8: The adaptive state feedback shared controller is designed specifically for constrained Non-Linear Mechanics systems.

IV. SIMULATION

Define the design parameters for the performance function as: $\psi_{\eta,0} = 5$, $\psi_{\tilde{T}_\eta} = 0.02$, $\lambda_\eta = 0.5$, $\tilde{T}_\eta = 9.1767$, $p_\eta = 5$, $d_\eta = 6$, $\tau_\eta = 5$, $m_\eta = 3$, $b_\eta = 5$, $\bar{b}_\eta = 7$, $l_\eta = 2$. Upon revisiting the definition of stability time, the following is derived: $\tilde{T}_\eta = \tilde{T}_V = 9.1767$. The chosen control design parameters are: $\psi_{V,0} = 5$, $\psi_{\tilde{T}_V} = 0.02$, $\lambda_V = 0.5$, $p_V = 5$, $d_V = 6$, $\tau_\eta = 5$, $m_V = 3$, $b_V = 5$, $\bar{b}_V = 7$, $\delta = 7$, $\rho = 5$, $l_V = 2$. By adjusting k_i, when $k_\eta = 0.3$ and $k_V = 0.3$, the transformation error is limited to a constant range of 0.3, thereby keeping the system within this stable region.

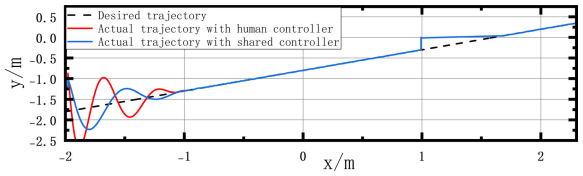

FIGURE 3. Tracking trajectory.

The definition of the convex feasible set is:

$$\mathrm{P}_{\alpha 1} = \left\{ p = \begin{bmatrix} x \\ y \\ \varphi \end{bmatrix} \middle| \begin{array}{c} -2 \leq x \leq -1; \\ -2.5 \leq y \leq 0.5; \\ -1.57 \leq \varphi \leq 1.57 \end{array} \right\} \tag{49}$$

Simulate the actions of a human operator driving the system within the set P_a. The model, exemplified by a system operated by a control lever, involves parameters such as $u_{h1} = 1$ and $u_{h1} = -1$, representing the rightmost and leftmost positions of the lever; $u_{h2} = 1$ and $u_{h2} = -1$, representing the uppermost and lowermost positions of the lever. For $u_{h3} = 1$, it signifies the maximum counterclockwise angle of the lever. Conversely, for $u_{h3} = -1$, it represents the maximum clockwise angle of the lever. The assumption is made that the actions of the individual impact the position of the control lever in the system. Taking a straight-line trajectory as the desired path for an unmanned surface vehicle, Simulation results are depicted in Fig. 3. It is apparent from the figure that in the task of straight-line trajectory tracking, within the setting, the red line indicates the use of solely human control input, violating convex constraints. Still, within the set, he blue line showcases the tracking outcomes in a straight-line manner, achieved through the utilization of the proposed shared controller, with no apparent violation of convex constraints in the graph.The adoption of the adaptive shared controller also enhances tracking performance. This suggests the effectiveness of the proposed shared controller in convex constraint scenarios.

The definition of the concave admissible set is:

$$\mathrm{P}_{\alpha 2} = \left\{ p = \begin{bmatrix} x \\ y \\ \varphi \end{bmatrix} \middle| \begin{array}{c} x \geq 1; \\ y \geq 0; \\ -1.57 \leq \varphi \leq 1.57 \end{array} \right\} \tag{50}$$

If the unmanned surface vehicle is under complete human control while attempting to perform straight-line trajectory tracking tasks, the unmanned surface vehicle's trajectory will enter an unacceptable region. However, when the unmanned surface vehicle utilizes a shared controller within the set $\mathrm{P}_{\alpha 2}$, the tracking task can still be accomplished under concave constraints.The figure demonstrates the unmanned surface vehicle's capability to navigate open constraints using the proposed shared controller, even in situations where its state is close to the boundary of $\mathrm{P}_{\alpha 2}$.This underscores the efficacy of the proposed shared controller in scenarios involving non-convex constraints.

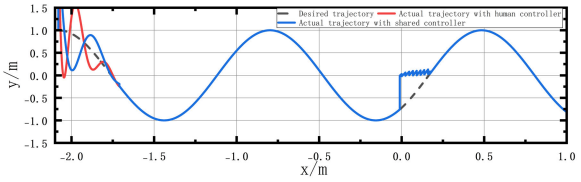

FIGURE 4. Tracking trajectory.

Assuming a non-straight line trajectory as the desired path for the omnidirectional mobile robot, the simulation results are depicted in Figure 4.

$$\mathrm{P}_{\alpha 3} = \left\{ p = \begin{bmatrix} x \\ y \\ \varphi \end{bmatrix} \middle| \begin{array}{c} -2.1 \le x \le -1.75; \\ -1.5 \le y \le 1.5; \\ -1.57 \le \varphi \le 1.57 \end{array} \right\} \tag{51}$$

$$\mathrm{P}_{\alpha 4} = \left\{ p = \begin{bmatrix} x \\ y \\ \varphi \end{bmatrix} \middle| \begin{array}{c} x \ge 0; \\ y \ge 0; \\ -1.57 \le \varphi \le 1.57 \end{array} \right\} \tag{52}$$

In Fig 4, it is observed that during the non-straight line trajectory tracking task within set $\mathrm{P}_{\alpha 3}$, the red line, representing the utilization of only human control input, distinctly violates convex constraints. Conversely, within set $\mathrm{P}_{\alpha 3}$, the blue line illustrates the trajectory tracking results using the proposed shared controller, showing no apparent violation of convex constraints in the graph. Additionally, the application of the adaptive shared controller enhances tracking performance. This underscores the efficacy of the proposed shared controller in scenarios involving convex constraints. Similarly, if the employs a shared controller within set $\mathrm{P}_{\alpha 4}$, the tracking task remains achievable even under concave constraints. The diagram highlights the effectiveness of the shared controller proposed in facilitating the unmanned surface vehicle's navigation through open constraints, even when its state approaches the boundary of set $\mathrm{P}_{\alpha 4}$.

The figures depict the tracking error trajectories for various control strategies, as shown in Figures 5 and 6. In Figure 5, the black line represents the error variation without PPC, where $|e_\eta|_{\max} > 0.025m$; the blue line represents the error variation with PPC, where $|e_\eta| < 0.015m$; and the yellow line represents the error variation with FTPPC, where $|e_\eta| < 0.001m$. In Figure 6, the black line represents the error variation without PPC, where $|e_\eta|_{\max} > 0.025m$; the blue line represents the error variation with PPC, where $|e_\eta| < 0.018m$; and the yellow line represents the error variation with FTPPC, where $|e_\eta| < 0.001m$.

Figures 5 and 6 illustrate the robust performance of the FTPPC algorithm, ensuring that both the tracking error and virtual error remain bounded while converging to the desired steady-state error within a predefined time frame. In contrast, the traditional PPC control method from [18] and the control algorithm without considering PPC from [19] exhibit tracking errors that exceed the performance bounds defined in this paper after a fixed time. Therefore, the innovative approach proposed in this paper demonstrates faster convergence

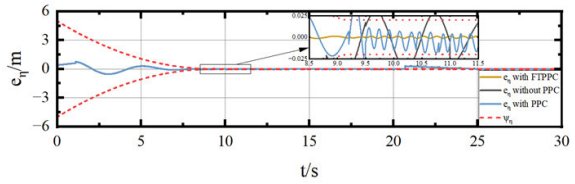

FIGURE 5. Tracking error e_η with different control strategies.

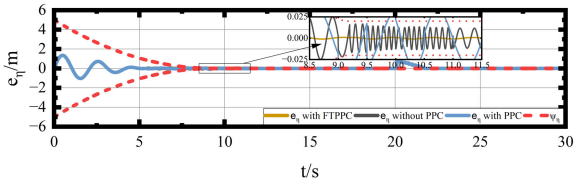

FIGURE 6. Tracking error e_η with different control strategies.

and exhibits superior constraint performance, ensuring the transient characteristics of the system.

V. CONCLUSION

This article mainly addresses the safety issues of unmanned surface vehicles in the face of emergencies. Firstly, an adaptive shared control system enables human operators and controllers to control inputs. Then, to make the tracking error converge, a pre-performance control function was designed to ensure the transient error of the tracking error. Secondly, a controller is created using the backstepping method, and Lyapunov functions are employed to verify the stability of the unmanned surface vehicle. Finally, a state feedback shared control function is designed to implement the shared control algorithm. Simulation results provide empirical evidence supporting the efficacy of the implemented control algorithm.

REFERENCES

[1] L. Cheng, B. Deng, Y. Yang, J. Lyu, J. Zhao, K. Zhou, C. Yang, L. Wang, S. Yang, and Y. He, "Water target recognition method and application for unmanned surface vessels," *IEEE Access*, vol. 10, pp. 421–434, 2022.

[2] M. Schiaretti, L. Chen, and R. R. Negenborn, "Survey on autonomous surface vessels: Part II—Categorization of 60 prototypes and future applications," in *Proc. 8th Int. Conf.*, 2017, pp. 234–252.

[3] A. Devaraju, L. Chen, and R. Negenborn, "Autonomous surface vessels in ports: Applications, technologies and port infrastructures," in *Proc. 9th Int. Conf. Comput. Logistics*, 2018, pp. 86–105.

[4] Z. Fang, J. Wang, Z. Wang, J. Liang, Y. Liu, and G. Yin, "A human-machine shared control framework considering time-varying driver characteristics," *IEEE Trans. Intell. Veh.*, vol. 8, no. 7, pp. 3826–3838, Jul. 2023.

[5] L. Zhou, Y. Dou, H. Liu, W. Zhang, J. Hu, and C. Yang, "Shared control method for coal mine rescue robots," in *Proc. 5th CAA Int. Conf. Veh. Control Intell. (CVCI)*, Oct. 2021, pp. 1–6.

[6] B. Varga, S. Hohmann, A. Shahirpour, M. Lemmer, and S. Schwab, "Limited-information cooperative shared control for vehicle-manipulators," in *Proc. IEEE Int. Conf. Syst. Man, Cybern. (SMC)*, Oct. 2020, pp. 4431–4438.

[7] H. Qin, C. Li, Y. Sun, X. Li, Y. Du, and Z. Deng, "Finite-time trajectory tracking control of unmanned surface vessel with error constraints and input saturations," *J. Franklin Inst.*, vol. 357, no. 16, pp. 11472–11495, Nov. 2020.

[8] M. Van, V.-T. Do, M. O. Khyam, and X. P. Do, "Tracking control of uncertain surface vessels with global finite-time convergence," *Ocean Eng.*, vol. 241, Dec. 2021, Art. no. 109974.

[9] N. Wang, H. R. Karimi, H. Li, and S.-F. Su, "Accurate trajectory tracking of disturbed surface vehicles: A finite-time control approach," *IEEE/ASME Trans. Mechatronics*, vol. 24, no. 3, pp. 1064–1074, Jun. 2019.

[10] J. Zhang, S. Yu, and Y. Yan, "Fixed-time extended state observer-based trajectory tracking and point stabilization control for marine surface vessels with uncertainties and disturbances," *Ocean Eng.*, vol. 186, Aug. 2019, Art. no. 106109.
[11] J. Zhang, S. Yu, D. Wu, and Y. Yan, "Nonsingular fixed-time terminal sliding mode trajectory tracking control for marine surface vessels with anti-disturbances," *Ocean Eng.*, vol. 217, Dec. 2020, Art. no. 108158.
[12] S. Song, J. H. Park, B. Zhang, and X. Song, "Event-triggered adaptive practical fixed-time trajectory tracking control for unmanned surface vehicle," *IEEE Trans. Circuits Syst. II, Exp. Briefs*, vol. 68, no. 1, pp. 436–440, Jan. 2021.
[13] C. P. Bechlioulis and G. A. Rovithakis, "Robust adaptive control of feedback linearizable MIMO nonlinear systems with prescribed performance," *IEEE Trans. Autom. Control*, vol. 53, no. 9, pp. 2090–2099, Oct. 2008.
[14] S.-L. Dai, S. He, M. Wang, and C. Yuan, "Adaptive neural control of underactuated surface vessels with prescribed performance guarantees," *IEEE Trans. Neural Netw. Learn. Syst.*, vol. 30, no. 12, pp. 3686–3698, Dec. 2019.
[15] J.-X. Zhang and T. Chai, "Singularity-free continuous adaptive control of uncertain underactuated surface vessels with prescribed performance," *IEEE Trans. Syst. Man, Cybern. Syst.*, vol. 52, no. 9, pp. 5646–5655, Sep. 2022.
[16] Z. Shen, Q. Wang, S. Dong, and H. Yu, "Dynamic surface control for tracking of unmanned surface vessel with prescribed performance and asymmetric time-varying full state constraints," *Ocean Eng.*, vol. 253, Jun. 2022, Art. no. 111319.
[17] Y. Li, S. Qiang, X. Zhuang, and O. Kaynak, "Robust and adaptive backstepping control for nonlinear systems using RBF neural networks," *IEEE Trans. Neural Netw.*, vol. 15, no. 3, pp. 693–701, May 2004.
[18] Y. Liu, X. Liu, Y. Jing, and Z. Zhang, "A novel finite-time adaptive fuzzy tracking control scheme for nonstrict feedback systems," *IEEE Trans. Fuzzy Syst.*, vol. 27, no. 4, pp. 646–658, Apr. 2019.
[19] D. Swaroop, J. K. Hedrick, P. P. Yip, and J. C. Gerdes, "Dynamic surface control for a class of nonlinear systems," *IEEE Trans. Autom. Control*, vol. 45, no. 10, Oct. 2000, Art. no. 18931899.
[20] X. Yang, W. Deng, and J. Yao, "Neural adaptive dynamic surface asymptotic tracking control of hydraulic manipulators with guaranteed transient performance," *IEEE Trans. Neural Netw. Learn. Syst.*, vol. 34, no. 10, pp. 7339–7349, Oct. 2023.
[21] X. Yang, Y. Ge, W. Deng, and J. Yao, "Command filtered adaptive tracking control of nonlinear systems with prescribed performance under time-variant parameters and input delay," *Int. J. Robust Nonlinear Control*, vol. 33, no. 4, pp. 2840–2860, Mar. 2023.
[22] Z. Ren, Y. Wang, D. Zaytsev, and V. Zaytsev, "Time-varying formation for MSVs with input and prescribed performance constraints by fixed-time event-triggered sliding mode control," *Ocean Eng.*, vol. 299, May 2024, Art. no. 117406.
[23] Z. Ren, T. Xia, and X. Wang, "Nonsingular terminal sliding mode-based distributed cooperative event-triggered control for multiple surface vessels under actuator faults with input saturation," *IEEE Access*, vol. 11, pp. 1115–1127, 2023.
[24] G. Xia and Z. Ren, "Event-triggered fixed-time distributed output feedback sliding mode cooperative control for multiple surface vessels with input saturation," *Trans. Inst. Meas. Control*, vol. 45, no. 15, pp. 2869–2889, Nov. 2023.
[25] Z. Ren and T. Xia, "Fixed-time output feedback distributed cooperative event-triggered control for multiple surface vessels with prescribed performance constraints," *IEEE Access*, vol. 11, pp. 15198–15210, 2023.

MENGYUE HE is currently pursuing the Bachelor of Engineering degree with Hubei University of Technology (HBUT), Wuhan. She is also pursuing her research under Dr. Wei Shang. She helped complete a few projects in the fields of shared control, stability analysis, and trajectory tracking.

CHAOBO LI is currently pursuing the B.Eng. degree with Hubei University of Technology (HBUT), Wuhan. He is currently pursuing his research under Dr. Wei Shang. He has completed a few projects in the fields of adaptive control and stability analysis.

HUA HUANG is currently pursuing the master's degree. He is also with Wuhan Railway Vocational and Technical College. His main research interests include control algorithm research and electric locomotive motors electrical control theory.

FANGFANG ZHOU is currently pursuing the bachelor's degree in engineering and technology with Hubei University of Technology (HBUT), Wuhan. She is pursuing her research under Dr. Wei Shang. She helped complete works on the unmanned ship's ground, including distributed control and dynamic compensator information acquisition to control the formation.

YUHANG HE is currently pursuing the Bachelor of Engineering degree with Hubei University of Technology (HBUT), Wuhan. He is also pursuing his research under Dr. Wei Shang. He has assisted in completing tasks related to shared control, stability analysis, and trajectory tracking.

WEI SHANG received the Ph.D. degree in aeronautical and astronautical science and technology from Beijing Institute of Technology, China, in 2017. He is currently a Lecturer with Hubei University of Technology. His research interests include control theory of multi-agent systems and fight control.